ACS Sustainable Chemistry & Engineering

Research Article

Cite This: ACS Sustainable Chem. Eng. 2019, 7, 4897−4902

pubs.acs.org/journal/ascecg

Microporous Metal−Organic Framework with Dual Functionalities for Efficient Separation of Acetylene from Light Hydrocarbon Mixtures

Hao Li,[†,‡] Libo Li,[‡,§] Rui-Biao Lin,[*,‡] Giorgio Ramirez,[‡] Wei Zhou,[∥] Rajamani Krishna,[⊥] Zhangjing Zhang,[†] Shengchang Xiang,[*,†] and Banglin Chen[*,‡]

[†]Fujian Provincial Key Laboratory of Polymer Materials, College of Materials Science and Engineering, Fujian Normal University, Fuzhou 350007, Fujian, People's Republic of China

[‡]Department of Chemistry, University of Texas at San Antonio, One UTSA Circle, San Antonio, Texas 78249-0698, United States

[§]College of Chemistry and Chemical Engineering, Taiyuan University of Technology, Taiyuan 030024, Shanxi, People's Republic of China

[∥]NIST Center for Neutron Research, National Institute of Standards and Technology, Gaithersburg, Maryland 20899-6102, United States

[⊥]Van 't Hoff Institute for Molecular Sciences, University of Amsterdam, Science Park 904, 1098 XH Amsterdam, The Netherlands

Supporting Information

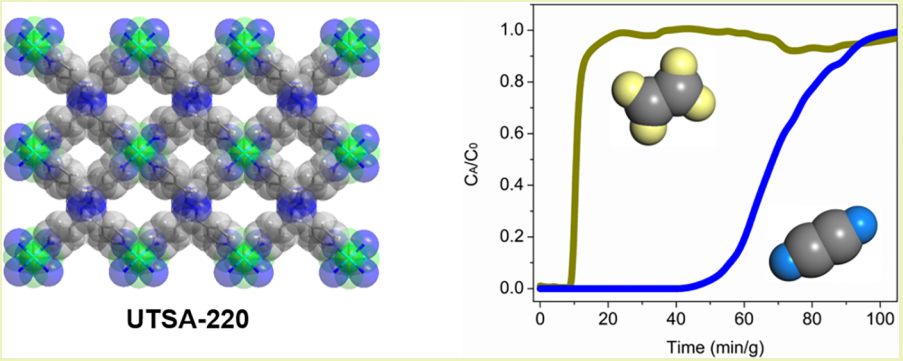

ABSTRACT: Separating acetylene from light hydrocarbon mixtures like ethylene is a very important process for downstream industrial applications. Herein, we report a new MOF $[CuL_2(SiF_6)]$ (UTSA-220, L = (1*E*,2*E*)-1,2-bis(pyridin-4-ylmethylene)hydrazine) with dual functionalities featuring optimal pore size with strong binding sites for acetylene. UTSA-220 exhibits apparently higher uptake capacity for C_2H_2 than those for other light hydrocarbons. The potential of this material for trace C_2H_2 removal from C_2H_4 has also been demonstrated by a dynamic breakthrough experiment performed with C_2H_2/C_2H_4 (1/99 v/v) under simulated industrial conditions. According to the dispersion-corrected density functional theory (DFT-D) simulation, SiF_6^{2-} and azine moieties serve as preferential binding sites for C_2H_2, indicating the feasibility of the dual functionalities incorporated in UTSA-220 for adsorbent-based C_2H_2 separations.

KEYWORDS: *Metal−organic frameworks, Light hydrocarbons, Gas separation, Acetylene*

INTRODUCTION

The separation of light hydrocarbons is widely regarded as important processes in petrochemistry.[1,2] Among them, acetylene (C_2H_2) is the source of many organic chemicals in industry, such as α-ethynyl alcohols, vinyl compounds, and acrylic acid derivatives.[3] C_2H_2 usually coexists with carbon dioxide (CO_2), ethylene (C_2H_4) or other light hydrocarbons, because C_2H_2 is mainly manufactured by cracking of hydrocarbons or partial combustion of methane (CH_4). Apart from this, C_2H_2 is a common impurity in the production of olefins like C_2H_4. The presence of C_2H_2 in C_2H_4 largely affects the downstream C_2H_4 polymerization reaction by poisoning the catalyst.[2] Thus, the significance of C_2H_2/C_2H_4 separation is comparable to that of some important separations such as C_2H_4/C_2H_6, C_3H_4/C_3H_6 and C_3H_6/C_3H_8.[4−8] Considerable difficulty has been encountered in the removal of C_2H_2 from the coexisting species for industrial requirements, because these small molecules are similar in physical properties such as molecular sizes, electronic structures, and volatilities.[9] Traditional cryogenic distillation method suffers

Received: October 23, 2018
Revised: January 8, 2019
Published: February 18, 2019

DOI: 10.1021/acssuschemeng.8b05480
ACS Sustainable Chem. Eng. 2019, 7, 4897−4902

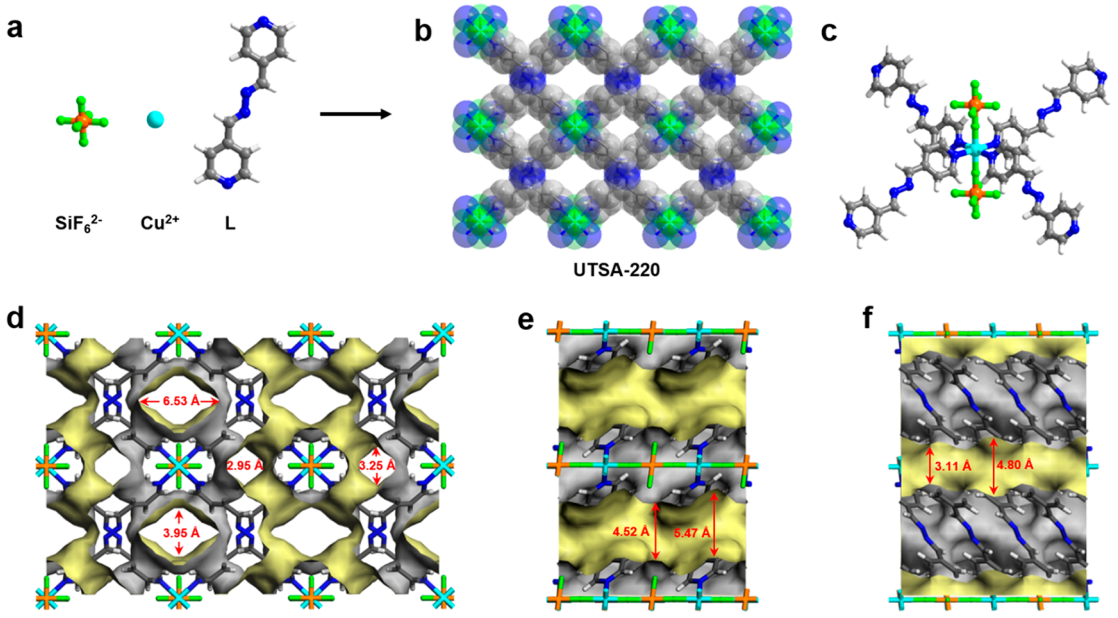

Figure 1. Building units (a) and structure (b) of UTSA-220. The channels of UTSA-220 are viewed along the *a*-axis. (c) The coordination sphere of Cu atom in UTSA-220. (d) Illustration of the channel dimensions of UTSA-220 viewed along the *a*-axis. Cross section of the larger (e) and smaller (f) channels viewed along *b*-axis. Color code: Cu, turquoise; F, bright green; Si, orange; C, gray; N, blue; H, white.

from the extraordinarily high energy and capital input, which propels us to develop alternative approaches to addressing the issue more efficiently.[1] Separation by means of adsorption with porous materials is perceived as a promising way to replace the traditional distillation method and has experienced significant development in recent years.[4−8,10−13]

As a new generation of porous materials, metal−organic frameworks (MOFs) have attracted vast attention in exploring their application potential in various fields,[14−21] including but not limited to gas storage,[22−25] separation,[6,26−34] catalysis,[35−38] sensing,[24,39,40] and drug delivery.[41,42] The diverse properties and functions of MOFs stem from their highly modifiable pore structure and surface.[43,44] With rational choice of the building blocks (metal ions/clusters and organic ligands), the topology, pore size, surface functionality of MOFs can be tailored specifically to fit into application scenarios like gas separation.[45,46] For C_2H_2 removal and enrichment, the control over pore size and pore functionalities are found effective in developing MOFs with desired performance.[8,47,48]

Recently, a series of MOFs containing SiF_6^{2-} moieties have been reported to have excellent abilities to separate C_2H_2 from C_2H_4 as a combined outcome of the molecular sieving effect and strong hydrogen bonding interactions between SiF_6^{2-} and C_2H_2 molecules.[8,49] Herein, we report a new MOF $[CuL_2(SiF_6)]$ (termed UTSA-220) based on an azine based ligand L (L = (1*E*,2*E*)-1,2-bis(pyridin-4-ylmethylene)-hydrazine), featuring a bifunctionalized environment for C_2H_2 accommodation in the framework. This MOF shows a three-dimensional (3D) network with one-dimensional (1D) channels that provide optimal pore size and strong binding sites for C_2H_2. Gas sorption studies reveal that UTSA-220 selectively adsorbs C_2H_2 over other light hydrocarbons at ambient temperature. A dynamic breakthrough experiment performed with a C_2H_2/C_2H_4 (1/99 v/v) mixture further demonstrates UTSA-220 is feasible to separate C_2H_2 from C_2H_4 under practical conditions.

EXPERIMENTAL SECTION

Synthesis of UTSA-220. Attempts to obtain single crystals were unsuccessful. Thus, bulk powder of this MOF was synthesized as follows. A methanolic solution of copper hexafluorosilicate was made by dissolving 22.4 mg (0.1 mmol) $CuSiF_6{\cdot}xH_2O$ into 10 mL methanol. The $CuSiF_6$ solution was added dropwise with constant stirring into a methanolic ligand solution prepared by dissolving 42 mg (0.2 mmol) L into 10 mL methanol. The suspension was stirred at room temperature for 30 min before the powder product was separated from the solution and washed with methanol for 3 times with a centrifuge. The product was transferred to a gas sorption tube and activated under vacuum at room temperature for 24 h before gas sorption measurements.

Breakthrough Experiment. The breakthrough experiments were conducted on a self-built instrument (see Supporting Information) with a gas mixture of C_2H_2/C_2H_4 (1/99 v/v) at room temperature (298 K) and 1 bar. The MOF solid was packed into a $\phi 2 \times 70$ mm stainless-steel column under the protection of N_2 gas in a glovebox. The packed column was flushed with helium gas at a rate of 40 mL/min for 2 h at room temperature to further activate the sample prior to measurements. The flow rate of the C_2H_2/C_2H_4 mixture was set at 2 mL/min and was first directed to a blank column to stabilize the gas flow before being switched to the adsorbent column to initiate the breakthrough experiment. The effluent composition was evaluated by a gas chromatography (GC) with a thermal conductivity detector (detection limit 0.1 ppm). Between two tests, the adsorbent was regenerated by helium flow (40 mL/min) for 12 h to guarantee a complete removal of the adsorbed gases. The desorption test on breakthrough instrument was performed at room temperature by switching the feed gas to He gas. The He flow was maintained at 20 mL/min. The effluent composition was measured by GC until no detectable C_2H_2 and C_2H_4 was found from the effluent.

RESULTS AND DISCUSSION

Structure and Synthesis. The dropwise addition of a methanolic solution of L ligand into a $CuSiF_6{\cdot}xH_2O$ methanolic solution at room temperature with constant stirring affords the light purple crystalline powder of UTSA-220. Based on its powder X-ray diffraction pattern, the rough structure of UTSA-220 was determined to crystallize in the space group of

DOI: 10.1021/acssuschemeng.8b05480
ACS Sustainable Chem. Eng. 2019, 7, 4897−4902

*C*2/*m* and has one Cu atom, in which two L ligands and one SiF_6 group were found in the asymmetric unit (Figure S1 and Table S1). In this MOF, Cu atom is coordinated by four N atoms equatorially and two F atoms axially (Figure 1a–c). The four N donors come from four bidentate L ligands while the two F atoms are from two bridging SiF_6^{2-} anions. The obtained structure is a 2-fold interpenetrated 3D network (Figure S2). Since the organic linker L is not parallel but tilted with respect to the axial direction of coordinated Cu^{2+} ion, UTSA-220 features two kinds of 1D channels along the *a*-axis (Figure 1b,d). Owing to interpenetration, the sizes of two channel windows are narrowed to 3.0 × 3.2 $Å^2$ and 4.0 × 6.5 $Å^2$ (Figure 1d), with the width of the larger channel between 4.5 and 5.5 Å and that of smaller one 3.1–4.8 Å (Figure 1e,f). The total guest-accessible volume for UTSA-220 is estimated to be 40%. The thermogravimetric analysis of the as-synthesized sample shows that the solvent molecules can be easily removed around ambient temperature, and framework decomposition is at around 250 °C (Figure S3).

Gas Sorption Properties. To investigate the porosity and channels in UTSA-220, the N_2 sorption isotherms at 77 K and CO_2 sorption at 195 K were collected. The obtained N_2 sorption curve is a typical type I isotherm with the Brunauer–Emmett–Teller (BET) and Langmuir surface areas as 577 and 825 m^2/g, respectively. With the aid of nonlocal density functional theory (NLDFT), the pore size distribution diagram was also obtained from the N_2 adsorption data, showing a narrow distribution of approximately 8.8 Å (Figure 2, inset).

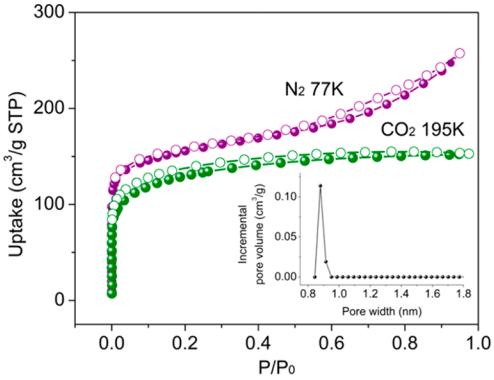

Figure 2. Gas sorption isotherms of UTSA-220. N_2 at 77 K (violet) and CO_2 at 195 K (olive). The inset graph shows its incremental pore size distribution obtained from N_2 isotherms at 77 K.

Notably, the measured pore volume of UTSA-220 is 0.35 cm^3/g based on 77 K N_2 isotherm (at P/P_0 = 0.85), which is consistent with the theoretical value of 0.33 cm^3/g from crystal structure, implying the well retention of its porosity. In contrast, the zinc analogue of UTSA-220 shows far lower measured pore volume,[50] which might be attributed to its high humidity sensitivity.

Because of the suitable pore size and favorably functionalized channels, UTSA-220 is suitable for selective adsorption of C_2H_2 over other light hydrocarbons. Gas sorption tests were performed on UTSA-220 at 298 K (Figure 3a) and 273 K (Figure S4) with C_2H_2, CO_2, C_2H_4, C_2H_6, CH_4 and N_2. UTSA-220 show distinct adsorption amount of these gases. At 298 K and 100 kPa (1 bar), C_2H_2 has the highest uptake (3.40 mmol/g) among the series, followed by CO_2 (3.38 mmol/g), C_2H_4 (2.53 mmol/g), C_2H_6 (2.14 mmol/g), CH_4 (0.59 mmol/g) and N_2 (0.18 mmol/g) (Figure 3a). At 273 K, the same sequence is also observed in corresponding gas uptakes (Figure S4). Dual-site Langmuir isotherm model was employed to fit the two sets of data at different temperatures to calculate the isosteric heat of adsorption (denoted as $-Q_{st}$) of these gases (Table S2). At zero-coverage, the $-Q_{st}$ for C_2H_2, CO_2, C_2H_4 and C_2H_6 are calculated to be 29, 27, 24 and 28 kJ/mol, respectively (Figure 3b). It should be noted that UTSA-220 adsorbs C_2H_2 rapidly at low pressure, with C_2H_2 uptake at 15 kPa reaching 2.40 mmol/g at 298 K. By contrast, the uptakes of CO_2 (1.56 mmol/g), C_2H_4 (1.22 mmol/g), C_2H_6 (1.10 mmol/g) and CH_4 (0.12 mmol/g) at the same condition are considerably lower. Such pronounced difference in the uptakes between C_2H_2 and other gas species reveals that UTSA-220 is very promising for C_2H_2 related separation. To assess the separation ability of UTSA-220, the ideal adsorbed solution theory (IAST) selectivity was calculated on the C_2H_2/C_2H_4 (1/99 v/v) and C_2H_2/CH_4 (1/99 v/v) mixtures (Figure 3c, Figure S5). The C_2H_2/C_2H_4 (1/99 v/v) adsorption selectivity at 100 kPa is 10, suggesting that UTSA-220 has the potential to effectively remove trace C_2H_2 from C_2H_4 to yield high quality monomer for polyethylene production. More impressively, the C_2H_2/CH_4 (1/99 v/v) selectivity is as high as 358 at 100 kPa (Table 1). We also calculate the equimolar IAST selectivity for C_2H_2/C_2H_4, C_2H_2/CO_2 and C_2H_2/C_2H_6 to explore the potential to perform C_2H_2 separation from these gas mixtures. Based on the results, UTSA-220 has moderately high selectivities in these separation scenarios, with the selectivity values as 8.8 (C_2H_2/C_2H_4), 4.4 (C_2H_2/CO_2) and 14 (C_2H_2/C_2H_6), respectively (Figure 3d, Table 1).

To delve into the adsorption mechanism of C_2H_2 and preferential C_2H_2 adsorption sites in UTSA-220, we carried out computational investigations using dispersion-corrected density functional theory (DFT-D). Two C_2H_2 adsorption sites are found within the framework, which are located at two different channels, respectively (Figure 4a). In Site I, C_2H_2 molecule is oriented almost parallel to the *c*-axis, with both hydrogen atoms pointing at two F atoms from two SiF_6^{2-} units. On both ends of the C_2H_2 molecule, the H···F distances are 1.994 Å (Figure 4b), suggesting C_2H_2 forms hydrogen bonds with the surrounding F atoms. In Site II, C_2H_2 molecule is almost parallel with the *ab* plane, and is in an orientation with both H in proximity to two F atoms. Since H···F distances are 2.420 Å (Figure 4c), the C_2H_2 molecule in Site II also has hydrogen bonds formed. Each C_2H_2 molecule interacts with two F atoms from SiF_6^{2-} units located on opposite sides of the channel simultaneously. The calculated static binding energies for two sites are −48.5 and −45.8 kJ/mol, respectively, which accounts for the highly selective adsorption of C_2H_2 over other light hydrocarbons. The adsorption of C_2H_2 follows the similar mechanism as those in previously reported SIFSIX MOFs,[8,49,51] which highly relies on the optimal pore structure that matches well with the molecular shape of C_2H_2. Moreover, the simulation at ambient pressure reveals that there exists an extra interaction between C_2H_2 and azine groups with modest strength in UTSA-220 (Figure S6). These simulation results serve as a good evidence for our rational design of the framework to achieve desired performance.

Breakthrough Experiment. To evaluate whether the material is capable to separate C_2H_2/C_2H_4 mixture in simulated industrial conditions, dynamic breakthrough experiments were conducted on UTSA-220 with a mixed gas of C_2H_2/C_2H_4 (1/99 v/v) using a homemade apparatus (Figure

DOI: 10.1021/acssuschemeng.8b05480
ACS Sustainable Chem. Eng. 2019, 7, 4897–4902

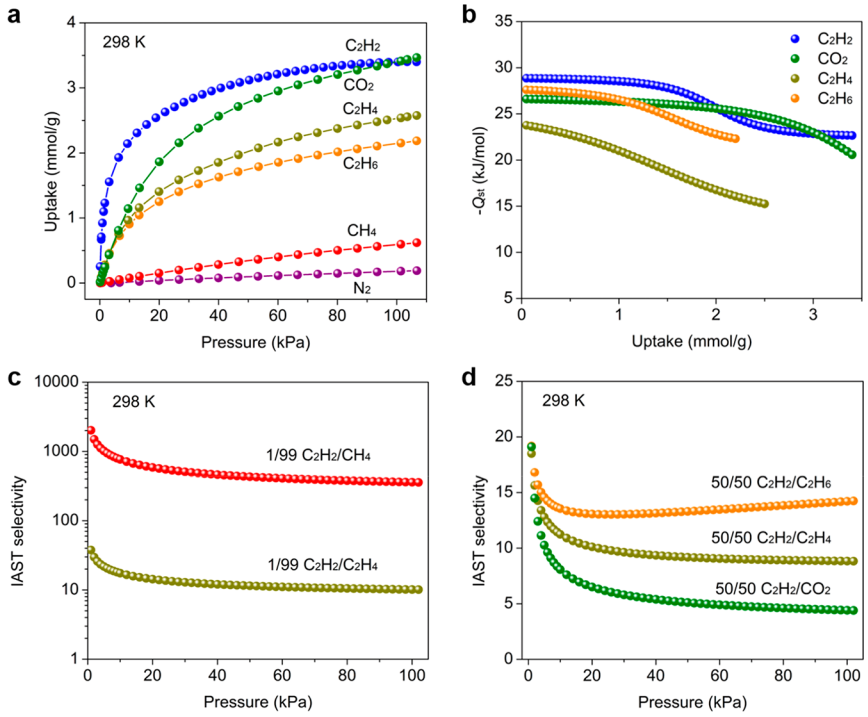

Figure 3. (a) C_2H_2, CO_2, C_2H_4, C_2H_6, CH_4 and N_2 adsorption isotherms of UTSA-220 at 298 K. (b) Isosteric heat of adsorption of C_2H_2, CO_2, C_2H_4, C_2H_6 in UTSA-220. (c) IAST selectivity of C_2H_2/CH_4 (1/99 v/v) and C_2H_2/C_2H_4 (1/99 v/v) at 298 K in UTSA-220. (d) IAST selectivity of C_2H_2/C_2H_6 (50/50 v/v), C_2H_2/C_2H_4 (50/50 v/v) and C_2H_2/CO_2 (50/50 v/v) at 298 K in UTSA-220.

Table 1. Summary of the IAST Selectivities of C_2H_2/C_2H_4 (1/99 v/v), C_2H_2/CH_4 (1/99 v/v), C_2H_2/C_2H_4 (50/50 v/v), C_2H_2/CO_2 (50/50 v/v) and C_2H_2/C_2H_6 (50/50 v/v) in UTSA-220 at 100 kPa

mixture	component proportion	IAST selectivity
C_2H_2/C_2H_4	1/99	10
C_2H_2/CH_4	1/99	358
C_2H_2/C_2H_4	50/50	8.8
C_2H_2/CO_2	50/50	4.4
C_2H_2/C_2H_6	50/50	14

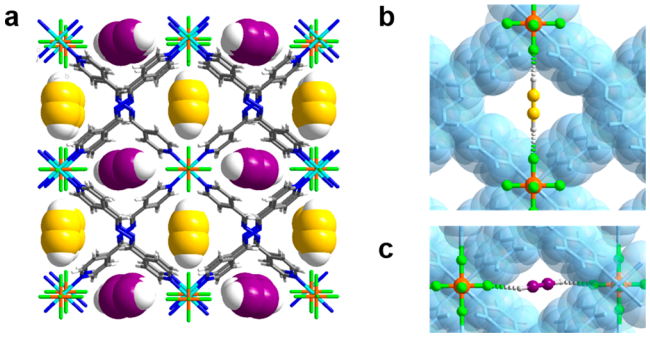

Figure 4. (a) DFT-D simulated adsorption sites for C_2H_2 in UTSA-220 and (b, c) their close contacts with the framework. Atom color code: F, bright green; Si, orange; Cu, turquoise; C in framework, gray; C in Site I, violet; C in Site II, golden; H, white; and N, blue.

S7) at a flow rate of 2 mL/min at 298 K and 1 bar. C_2H_4 was first monitored at the column outlet after a short period of time since the start of the experiment, while C_2H_2 was still fully captured by the adsorbent and retained in the column (Figure 5). At this stage, a polymer-grade pure C_2H_4 was generated from the column with no measurable C_2H_2 (<0.1 ppm),

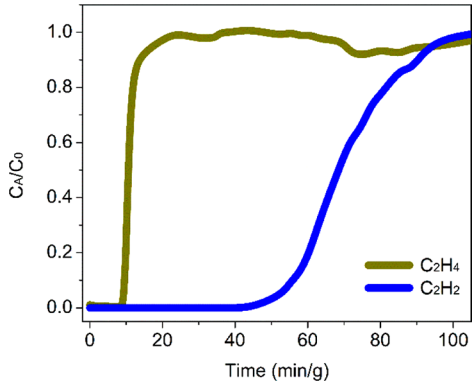

Figure 5. Experimental column breakthrough curves of UTSA-220 material for C_2H_2/C_2H_4 (1/99 v/v) separation at 298 K and 1 bar.

indicating UTSA-220 is effective to remove trace amount of C_2H_2 from C_2H_4. As the adsorbent was close to saturation, C_2H_2 emerged from the column and gradually increased in concentration until all C_2H_2 in the gas mixture can be probed. The retention time for C_2H_2 and C_2H_4 are 48 min/g and 10 min/g, respectively. In order to test whether UTSA-220 can be utilized as a reusable adsorbent, the column was successively regenerated using a He flow at a rate of 20 mL/min at room temperature and put to breakthrough experiments for four times (Figures S8 and S9). Each time, breakthrough time is around 48 min/g, suggesting the recyclable feature of UTSA-220.

CONCLUSION

To sum up, a new MOF with dual functionalities was successfully synthesized based on an azine ligand (1*E*,2*E*)-1,2-bis(pyridin-4-ylmethylene)hydrazine for efficient C_2H_2 remov-

DOI: 10.1021/acssuschemeng.8b05480
ACS Sustainable Chem. Eng. 2019, 7, 4897−4902

al and purification. Thanks to the dual functionalities, this MOF exhibits selective adsorption of C_2H_2 over other light hydrocarbons like C_2H_4. Breakthrough experiments further demonstrate the feasibility to remove trace amount of C_2H_2 from a mixture of C_2H_2 and C_2H_4 with this MOF as the column adsorbent. This work affords a functionalized approach of novel porous materials to advancing important gas separations in relevant energy-intensive petrochemical processes.

■ ASSOCIATED CONTENT

Supporting Information

The Supporting Information is available free of charge on the ACS Publications website at DOI: 10.1021/acssuschemeng.8b05480.

Sample preparation, data collection and analysis (PDF)

■ AUTHOR INFORMATION

Corresponding Authors

*B. Chen. Email: banglin.chen@utsa.edu.
*S. Xiang. Email: scxiang@fjnu.edu.cn.
*R.-B. Lin. Email: ruibiao.lin@utsa.edu.

ORCID

Rui-Biao Lin: 0000-0003-3267-220X
Wei Zhou: 0000-0002-5461-3617
Rajamani Krishna: 0000-0002-4784-8530
Shengchang Xiang: 0000-0001-6016-2587
Banglin Chen: 0000-0001-8707-8115

Notes

The authors declare no competing financial interest.

■ ACKNOWLEDGMENTS

We gratefully acknowledge the financial support from National Natural Science Foundation of China (21673039, 21573042, 21606163), Fujian Science and Technology Department (2018J07001), Foundation of State Key Laboratory of Coal Conversion (J18-19-610) and the Welch Foundation (AX-1730). We also thank Dr. Shengfei Jin for his help in packing UTSA-220 into the breakthrough column in a glovebox.

■ REFERENCES

(1) Yang, S.; Ramirez-Cuesta, A. J.; Newby, R.; Garcia-Sakai, V.; Manuel, P.; Callear, S. K.; Campbell, S. I.; Tang, C. C.; Schröder, M. Supramolecular binding and separation of hydrocarbons within a functionalized porous metal−organic framework. *Nat. Chem.* **2015**, *7*, 121−129.

(2) Bao, Z.; Chang, G.; Xing, H.; Krishna, R.; Ren, Q.; Chen, B. Potential of microporous metal−organic frameworks for separation of hydrocarbon mixtures. *Energy Environ. Sci.* **2016**, *9* (12), 3612−3641.

(3) Pässler, P.; Hefner, W.; Buckl, K.; Meinass, H.; Meiswinkel, A.; Wernicke, H.-J.; Ebersberg, G.; Müller, R.; Bässler, J.; Behringer, H.; Mayer, D. *Ullmann's encyclopedia of industrial chemistry*; Wiley-VCH: Weinheim, Germany, 2000; DOI: 10.1002/14356007.

(4) Lin, R.-B.; Li, L.; Zhou, H.-L.; Wu, H.; He, C.; Li, S.; Krishna, R.; Li, J.; Zhou, W.; Chen, B. Molecular sieving of ethylene from ethane using a rigid metal−organic framework. *Nat. Mater.* **2018**, *17* (12), 1128−1133.

(5) Li, L.; Lin, R.-B.; Krishna, R.; Li, H.; Xiang, S.; Wu, H.; Li, J.; Zhou, W.; Chen, B. Ethane/ethylene separation in a metal-organic framework with iron-peroxo sites. *Science* **2018**, *362* (6413), 443−446.

(6) Cadiau, A.; Adil, K.; Bhatt, P. M.; Belmabkhout, Y.; Eddaoudi, M. A metal-organic framework−based splitter for separating propylene from propane. *Science* **2016**, *353* (6295), 137−140.

(7) Li, L.; Lin, R.-B.; Krishna, R.; Wang, X.; Li, B.; Wu, H.; Li, J.; Zhou, W.; Chen, B. Flexible−robust metal−organic framework for efficient removal of propyne from propylene. *J. Am. Chem. Soc.* **2017**, *139* (23), 7733−7736.

(8) Cui, X.; Chen, K.; Xing, H.; Yang, Q.; Krishna, R.; Bao, Z.; Wu, H.; Zhou, W.; Dong, X.; Han, Y.; Li, B.; Ren, Q.; Zaworotko, M. J.; Chen, B. Pore chemistry and size control in hybrid porous materials for acetylene capture from ethylene. *Science* **2016**, *353* (6295), 141−144.

(9) Zhao, X.; Wang, Y.; Li, D.-S.; Bu, X.; Feng, P. Metal−organic frameworks for separation. *Adv. Mater.* **2018**, *30* (37), 1705189.

(10) Adil, K.; Belmabkhout, Y.; Pillai, R. S.; Cadiau, A.; Bhatt, P. M.; Assen, A. H.; Maurin, G.; Eddaoudi, M. Gas/vapour separation using ultra-microporous metal-organic frameworks: insights into the structure/separation relationship. *Chem. Soc. Rev.* **2017**, *46* (11), 3402−3430.

(11) Lin, R.-B.; Wu, H.; Li, L.; Tang, X.-L.; Li, Z.; Gao, J.; Cui, H.; Zhou, W.; Chen, B. Boosting ethane/ethylene separation within isoreticular ultramicroporous metal−organic frameworks. *J. Am. Chem. Soc.* **2018**, *140* (40), 12940−12946.

(12) Lin, R.-B.; Xiang, S.; Xing, H.; Zhou, W.; Chen, B. Exploration of porous metal−organic frameworks for gas separation and purification. *Coord. Chem. Rev.* **2019**, *378*, 87−103.

(13) Poliakoff, M.; Licence, P. Green chemistry. *Nature* **2007**, *450*, 810−812.

(14) Furukawa, H.; Cordova, K. E.; O'Keeffe, M.; Yaghi, O. M. The chemistry and applications of metal-organic frameworks. *Science* **2013**, *341* (6149), 1230444.

(15) Zhou, H.-C. J.; Kitagawa, S. Metal−organic frameworks (MOFs). *Chem. Soc. Rev.* **2014**, *43* (16), 5415−5418.

(16) Kitagawa, S.; Kitaura, R.; Noro, S.-i. Functional porous coordination polymers. *Angew. Chem., Int. Ed.* **2004**, *43* (18), 2334−2375.

(17) Wang, C.; Liu, D.; Lin, W. Metal−organic frameworks as a tunable platform for designing functional molecular materials. *J. Am. Chem. Soc.* **2013**, *135* (36), 13222−13234.

(18) Nugent, P.; Belmabkhout, Y.; Burd, S. D.; Cairns, A. J.; Luebke, R.; Forrest, K.; Pham, T.; Ma, S.; Space, B.; Wojtas, L.; Eddaoudi, M.; Zaworotko, M. J. Porous materials with optimal adsorption thermodynamics and kinetics for CO_2 separation. *Nature* **2013**, *495*, 80−84.

(19) Zhu, Q.-L.; Xu, Q. Metal−organic framework composites. *Chem. Soc. Rev.* **2014**, *43* (16), 5468−5512.

(20) Zhou, H.-C.; Long, J. R.; Yaghi, O. M. Introduction to metal−organic frameworks. *Chem. Rev.* **2012**, *112* (2), 673−674.

(21) Petit, C.; Bandosz, T. J. MOF−graphite oxide composites: combining the uniqueness of graphene layers and metal−organic frameworks. *Adv. Mater.* **2009**, *21* (46), 4753−4757.

(22) Cui, Y.; Li, B.; He, H.; Zhou, W.; Chen, B.; Qian, G. Metal−organic frameworks as platforms for functional materials. *Acc. Chem. Res.* **2016**, *49* (3), 483−493.

(23) He, Y.; Zhou, W.; Qian, G.; Chen, B. Methane storage in metal−organic frameworks. *Chem. Soc. Rev.* **2014**, *43* (16), 5657−5678.

(24) Chen, B.; Xiang, S.; Qian, G. Metal−organic frameworks with functional pores for recognition of small molecules. *Acc. Chem. Res.* **2010**, *43* (8), 1115−1124.

(25) Li, H.; Wang, K.; Sun, Y.; Lollar, C. T.; Li, J.; Zhou, H.-C. Recent advances in gas storage and separation using metal−organic frameworks. *Mater. Today* **2018**, *21* (2), 108−121.

(26) Bloch, E. D.; Queen, W. L.; Krishna, R.; Zadrozny, J. M.; Brown, C. M.; Long, J. R. Hydrocarbon separations in a metal-organic framework with open iron(II) coordination sites. *Science* **2012**, *335* (6076), 1606−1610.

(27) Foo, M. L.; Matsuda, R.; Hijikata, Y.; Krishna, R.; Sato, H.; Horike, S.; Hori, A.; Duan, J.; Sato, Y.; Kubota, Y.; Takata, M.;

DOI: 10.1021/acssuschemeng.8b05480
ACS Sustainable Chem. Eng. 2019, 7, 4897−4902

Kitagawa, S. An adsorbate discriminatory gate effect in a flexible porous coordination polymer for selective adsorption of CO_2 over C_2H_2. *J. Am. Chem. Soc.* **2016**, *138* (9), 3022−3030.
(28) Hamon, L.; Llewellyn, P. L.; Devic, T.; Ghoufi, A.; Clet, G.; Guillerm, V.; Pirngruber, G. D.; Maurin, G.; Serre, C.; Driver, G.; van Beek, W.; Jolimaître, E.; Vimont, A.; Daturi, M.; Férey, G. Co-adsorption and separation of CO_2−CH_4 mixtures in the highly flexible MIL-53(Cr) MOF. *J. Am. Chem. Soc.* **2009**, *131* (47), 17490−17499.
(29) Howarth, A. J.; Katz, M. J.; Wang, T. C.; Platero-Prats, A. E.; Chapman, K. W.; Hupp, J. T.; Farha, O. K. High efficiency adsorption and removal of selenate and selenite from water using metal−organic frameworks. *J. Am. Chem. Soc.* **2015**, *137* (23), 7488−7494.
(30) Luo, F.; Yan, C.; Dang, L.; Krishna, R.; Zhou, W.; Wu, H.; Dong, X.; Han, Y.; Hu, T.-L.; O'Keeffe, M.; Wang, L.; Luo, M.; Lin, R.-B.; Chen, B. UTSA-74: a MOF-74 isomer with two accessible binding sites per metal center for highly selective gas separation. *J. Am. Chem. Soc.* **2016**, *138* (17), 5678−5684.
(31) Liao, P.-Q.; Huang, N.-Y.; Zhang, W.-X.; Zhang, J.-P.; Chen, X.-M. Controlling guest conformation for efficient purification of butadiene. *Science* **2017**, *356* (6343), 1193−1196.
(32) Gelfand, B. S.; Huynh, R. P. S.; Mah, R. K.; Shimizu, G. K. H. Mediating order and modulating porosity by controlled hydrolysis in a phosphonate monoester metal−organic framework. *Angew. Chem., Int. Ed.* **2016**, *55* (47), 14614−14617.
(33) Thallapally, P. K.; Tian, J.; Radha Kishan, M.; Fernandez, C. A.; Dalgarno, S. J.; McGrail, P. B.; Warren, J. E.; Atwood, J. L. Flexible (breathing) interpenetrated metal−organic frameworks for CO_2 separation applications. *J. Am. Chem. Soc.* **2008**, *130* (50), 16842−16843.
(34) Rodenas, T.; Luz, I.; Prieto, G.; Seoane, B.; Miro, H.; Corma, A.; Kapteijn, F.; Llabrés i Xamena, F. X.; Gascon, J. Metal−organic framework nanosheets in polymer composite materials for gas separation. *Nat. Mater.* **2015**, *14*, 48−55.
(35) Lu, G.; Li, S.; Guo, Z.; Farha, O. K.; Hauser, B. G.; Qi, X.; Wang, Y.; Wang, X.; Han, S.; Liu, X.; DuChene, J. S.; Zhang, H.; Zhang, Q.; Chen, X.; Ma, J.; Loo, S. C. J.; Wei, W. D.; Yang, Y.; Hupp, J. T.; Huo, F. Imparting functionality to a metal−organic framework material by controlled nanoparticle encapsulation. *Nat. Chem.* **2012**, *4*, 310−316.
(36) Li, B.; Chrzanowski, M.; Zhang, Y.; Ma, S. Applications of metal-organic frameworks featuring multi-functional sites. *Coord. Chem. Rev.* **2016**, *307*, 106−129.
(37) Li, B.; Leng, K.; Zhang, Y.; Dynes, J. J.; Wang, J.; Hu, Y.; Ma, D.; Shi, Z.; Zhu, L.; Zhang, D.; Sun, Y.; Chrzanowski, M.; Ma, S. Metal−organic framework based upon the synergy of a Brønsted acid framework and Lewis acid centers as a highly efficient heterogeneous catalyst for fixed-bed reactions. *J. Am. Chem. Soc.* **2015**, *137* (12), 4243−4248.
(38) Gascon, J.; Corma, A.; Kapteijn, F.; Llabrés i Xamena, F. X. Metal organic framework catalysis: quo vadis? *ACS Catal.* **2014**, *4* (2), 361−378.
(39) Hu, Z.; Deibert, B. J.; Li, J. Luminescent metal−organic frameworks for chemical sensing and explosive detection. *Chem. Soc. Rev.* **2014**, *43* (16), 5815−5840.
(40) Zhang, M.; Feng, G.; Song, Z.; Zhou, Y.-P.; Chao, H.-Y.; Yuan, D.; Tan, T. T. Y.; Guo, Z.; Hu, Z.; Tang, B. Z.; Liu, B.; Zhao, D. Two-dimensional metal−organic framework with wide channels and responsive turn-on fluorescence for the chemical sensing of volatile organic compounds. *J. Am. Chem. Soc.* **2014**, *136* (20), 7241−7244.
(41) Horcajada, P.; Gref, R.; Baati, T.; Allan, P. K.; Maurin, G.; Couvreur, P.; Férey, G.; Morris, R. E.; Serre, C. Metal−organic frameworks in biomedicine. *Chem. Rev.* **2012**, *112* (2), 1232−1268.
(42) Zhao, D.; Tan, S.; Yuan, D.; Lu, W.; Rezenom, Y. H.; Jiang, H.; Wang, L.-Q.; Zhou, H.-C. Surface functionalization of porous coordination nanocages via click chemistry and their application in drug delivery. *Adv. Mater.* **2011**, *23* (1), 90−93.
(43) Bai, Y.; Dou, Y.; Xie, L.-H.; Rutledge, W.; Li, J.-R.; Zhou, H.-C. Zr-based metal−organic frameworks: design, synthesis, structure, and applications. *Chem. Soc. Rev.* **2016**, *45* (8), 2327−2367.
(44) Zhang, Y.-B.; Furukawa, H.; Ko, N.; Nie, W.; Park, H. J.; Okajima, S.; Cordova, K. E.; Deng, H.; Kim, J.; Yaghi, O. M. Introduction of functionality, selection of topology, and enhancement of gas adsorption in multivariate metal−organic framework-177. *J. Am. Chem. Soc.* **2015**, *137* (7), 2641−2650.
(45) Wang, H.; Dong, X.; Lin, J.; Teat, S. J.; Jensen, S.; Cure, J.; Alexandrov, E. V.; Xia, Q.; Tan, K.; Wang, Q.; Olson, D. H.; Proserpio, D. M.; Chabal, Y. J.; Thonhauser, T.; Sun, J.; Han, Y.; Li, J. Topologically guided tuning of Zr-MOF pore structures for highly selective separation of C6 alkane isomers. *Nat. Commun.* **2018**, *9* (1), 1745.
(46) Horike, S.; Inubushi, Y.; Hori, T.; Fukushima, T.; Kitagawa, S. A solid solution approach to 2D coordination polymers for CH_4/CO_2 and CH_4/C_2H_6 gas separation: equilibrium and kinetic studies. *Chem. Sci.* **2012**, *3* (1), 116−120.
(47) Hu, T.-L.; Wang, H.; Li, B.; Krishna, R.; Wu, H.; Zhou, W.; Zhao, Y.; Han, Y.; Wang, X.; Zhu, W.; Yao, Z.; Xiang, S.; Chen, B. Microporous metal−organic framework with dual functionalities for highly efficient removal of acetylene from ethylene/acetylene mixtures. *Nat. Commun.* **2015**, *6*, 7328.
(48) Li, L.; Lin, R.-B.; Krishna, R.; Wang, X.; Li, B.; Wu, H.; Li, J.; Zhou, W.; Chen, B. Efficient separation of ethylene from acetylene/ethylene mixtures by a flexible-robust metal−organic framework. *J. Mater. Chem. A* **2017**, *5* (36), 18984−18988.
(49) Li, B.; Cui, X.; O'Nolan, D.; Wen, H.-M.; Jiang, M.; Krishna, R.; Wu, H.; Lin, R.-B.; Chen, Y.-S.; Yuan, D.; Xing, H.; Zhou, W.; Ren, Q.; Qian, G.; Zaworotko, M. J.; Chen, B. An ideal molecular sieve for acetylene removal from ethylene with record selectivity and productivity. *Adv. Mater.* **2017**, *29* (47), 1704210.
(50) Manna, B.; Sharma, S.; Ghosh, S. Synthesis and crystal structure of a Zn(II)-based MOF bearing neutral n-donor linker and SiF_6^{2-} anion. *Crystals* **2018**, *8* (1), 37.
(51) Lin, R.-B.; Li, L.; Wu, H.; Arman, H.; Li, B.; Lin, R.-G.; Zhou, W.; Chen, B. Optimized separation of acetylene from carbon dioxide and ethylene in a microporous material. *J. Am. Chem. Soc.* **2017**, *139* (23), 8022−8028.

DOI: 10.1021/acssuschemeng.8b05480
ACS Sustainable Chem. Eng. 2019, 7, 4897−4902

Supporting Information

A microporous metal-organic framework with dual functionalities for efficient separation of acetylene from light hydrocarbon mixtures

Hao Li,[ab] Libo Li,[bc] Rui-Biao Lin,[b]* Giorgio Ramirez,[b] Wei Zhou,[d] Rajamani Krishna,[e] Zhangjing Zhang,[a] Shengchang Xiang,[a]* and Banglin Chen[b]*

[a] *Fujian Provincial Key Laboratory of Polymer Materials, College of Materials Science and Engineering, Fujian Normal University, Fuzhou 350007, Fujian, P. R. China.*

[b] *Department of Chemistry, University of Texas at San Antonio, One UTSA Circle, San Antonio, TX 78249-0698, United States*

[c] *College of Chemistry and Chemical Engineering, Taiyuan University of Technology, Taiyuan 030024, Shanxi, P. R. China.*

[d] *NIST Center for Neutron Research, National Institute of Standards and Technology, Gaithersburg, MD 20899-6102, United States*

[e] *Van 't Hoff Institute for Molecular Sciences, University of Amsterdam, Science Park 904, 1098 XH Amsterdam, Netherlands*

*To whom correspondence should be addressed:

Prof. Banglin Chen banglin.chen@utsa.edu;

Prof. Shengchang Xiang scxiang@fjnu.edu.cn;

Dr. Rui-Biao Lin ruibiao.lin@utsa.edu

Total number of pages: 15
Total number of figures: 9
Total number of tables: 2
Total number of equations: 5

Table of Contents

Chemicals

4-pyridinecarboxaldehyde, methanol, ethanol, acetic acid, hydrazine hydrate, copper hexafluorosilicate hydrate were purchased from Fisher Scientific. All commercial chemicals were used without further purification unless otherwise mentioned. Compressed He, C_2H_2, CO_2, C_2H_4, C_2H_6, CH_4, C_3H_6, C_3H_8, N_2, and C_2H_2/C_2H_4 (1/99 v/v) gases were bought from Airgas.

Instruments

Powder X-ray diffraction (PXRD) was carried out with a BRUKER D8-Focus Bragg-Brentano X-ray Powder Diffractometer equipped with a Cu sealed tube (λ = 1.54178 Å) at 40 kV and 40 mA. Gas sorption isotherms were measured using a Micromeritics ASAP 2020 system at various temperatures. ThermoFisher water bath is used to keep the BET sample tube at a constant temperature of 273 or 298 K. Thermogravimetric analysis (TGA) was carried out using a Shimadzu TGA-50 analyzer.

Synthesis of (1*E*,2*E*)-1,2-bis(pyridin-4-ylmethylene)hydrazine (L)

Linker L was synthesized according to a reported procedure.[1] 4.7 mL 4-pyridinecarboxaldehyde (49.94 mmol) was charged into a round bottomed flask. To this flask a mixed solvent made by 15 mL methanol and 15 mL ethanol and a catalytic quantity of acetic acid were added successively. This mixture was stirred at 120 °C for 0.5 h. Afterwards, 0.970 mL hydrazine hydrate (19.97 mmol) was added and the mixture was maintained at 120 °C with constant stirring for 12 h. Yellow crystalline product was generated after the reaction was cooled down to room temperature. The

crude product was recrystallized from a combined solvent of 1:1(v/v) methanol:ethanol. Yield ~ 85%

Gas sorption measurement

To remove all the guest solvents in the framework, the fresh as-synthesized sample of UTSA-220 was guest-exchanged with methanol at least 5 times. The sample was degassed at room temperature until the outgas rate was 5 μmHg/min prior to measurements. C_2H_2, CO_2, C_2H_4, C_2H_6, CH_4, C_3H_6, C_3H_8 and N_2 adsorption isotherms were collected on Micromeritics ASAP 2020 surface area analyzer for the guest-free sample. Pore size distribution (PSD) data were obtained from the 77 K N_2 adsorption isotherm based on the no-local density functional theory (NLDFT) model.

Framework structure

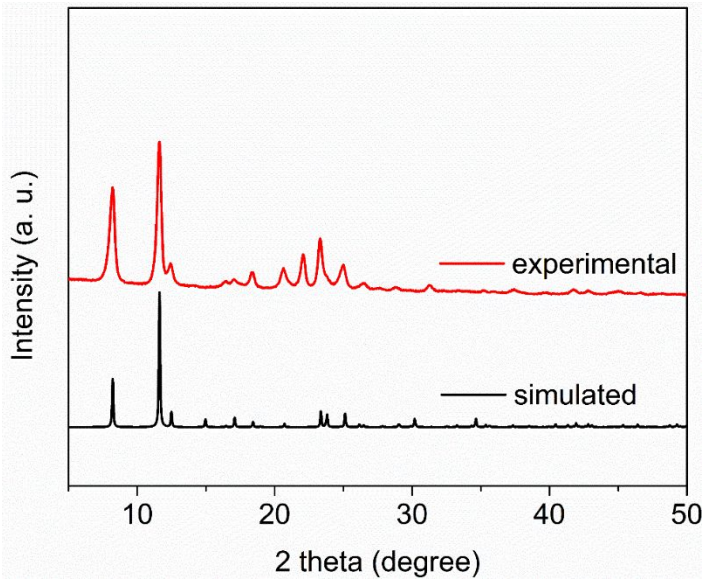

Figure S1. Experimental and simulated powder X-ray diffraction (PXRD) patterns of UTSA-220. The slight difference at around 20° can be attributed to the framework flexibility associated with the evaporation of volatile guest solvent molecules from this MOF during the test.

Table S1. Lattice parameters of the modeled structure of UTSA-220.

Empirical formula[a]	$C_{48}H_{40}N_{16}F_{12}Cu_2Si_2$
Formula weight	1252.24
T (K)	298
Crystal system	monoclinic
Space group	*C2/m*
a /Å	7.500
b /Å	21.520
c /Å	10.760
β (°)	90
Volume /Å^3	1736.7
Z	2
Density /g/cm^3	1.197

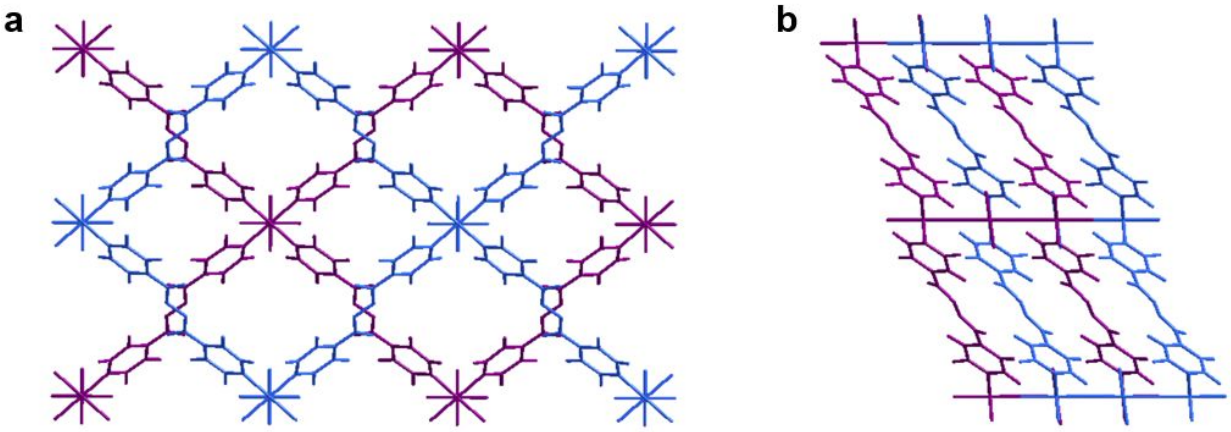

Figure S2. Illustration of the two-fold interpenetration structures of UTSA-220, viewed along *a*-axis and *b*-axis, respectively.

TGA experiment

TGA experiment was conducted using a Shimadzu TGA-50 analyzer. 7.82 mg UTSA-220 sample was placed in a platinum pan under N_2 atmosphere with a flow rate of 30 mL/min. The temperature was raised from room temperature to 780 °C at a heating rate of 10 °C/min.

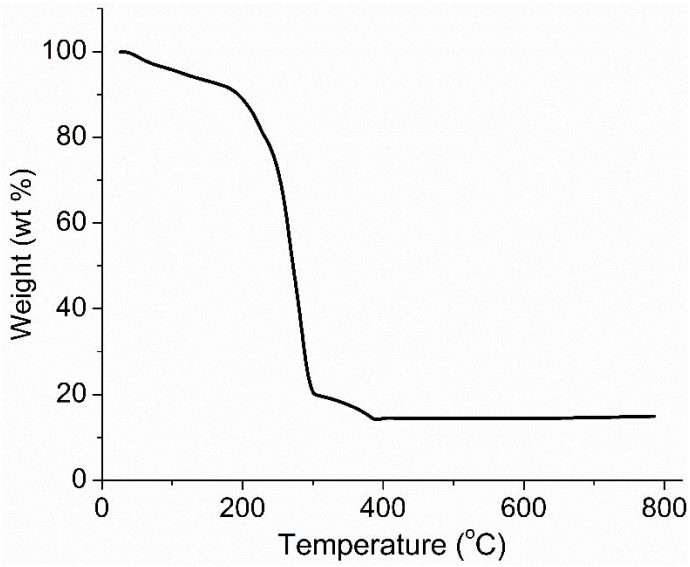

Figure S3. Thermogravimetric analysis UTSA-220 performed with N_2 flow.

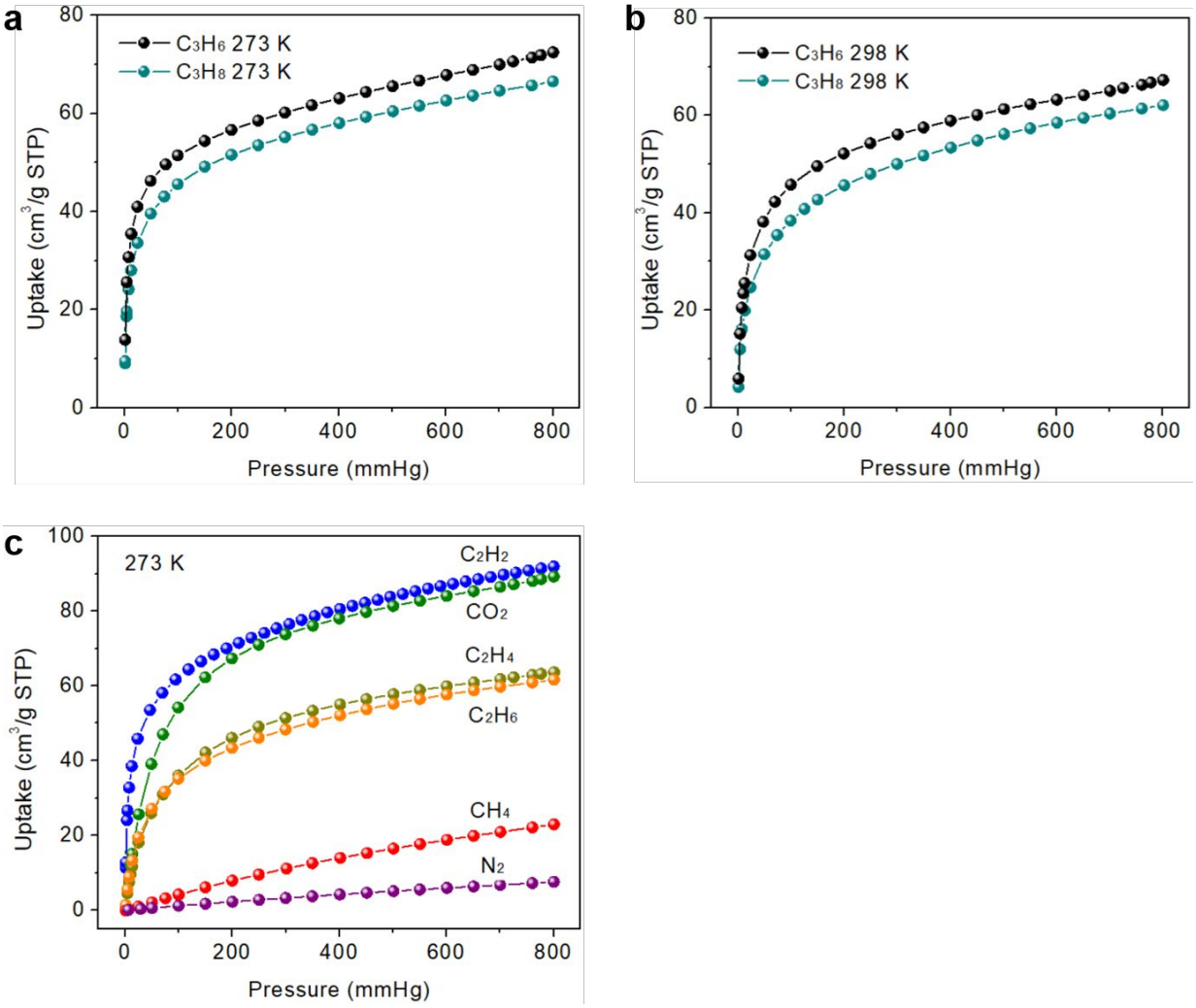

Figure S4. Adsorption isotherms of C_3H_6 and C_3H_8 in UTSA-220 at (a) 273 K and (b) 298 K. (c) C_2H_2, CO_2, C_2H_4, C_2H_6, CH_4, and N_2 adsorption isotherms of UTSA-220 at 273 K.

Isosteric heat of adsorption

The pure component isotherm data for C_2H_2, CO_2, C_2H_4, and C_2H_6, measured at 273 K, and 298 K were fitted with the dual-site Langmuir isotherm model.

$$q = q_{A,sat}\frac{b_A p}{1+b_A p} + q_{B,sat}\frac{b_B p}{1+b_B p} \quad \textbf{(Equation S1)}$$

with T-dependent parameters b_A, and b_B

$$b_A = b_{A0}\exp\left(\frac{E_A}{RT}\right); \quad b_B = b_{B0}\exp\left(\frac{E_B}{RT}\right) \quad \textbf{(Equation S2)}$$

The dual-site Langmuir parameters are provided in **Table S2**

The binding energy of C_2H_2 is reflected in the isosteric heat of adsorption, $-Q_{st}$, defined as

$$Q_{st} = RT^2\left(\frac{\partial \ln p}{\partial T}\right)_q \quad \textbf{(Equation S3)}$$

Table S2. T-dependent dual-site Langmuir fit parameters for C_2H_2, CO_2, C_2H_4, and C_2H_6.

	Site A			Site B		
	$q_{A,sat}$ (mol kg^{-1})	b_{A0} (Pa^{-1})	E_A (kJ mol^{-1})	$q_{B,sat}$ (mol kg^{-1})	b_{B0} (Pa^{-1})	E_B (kJ mol^{-1})
C_2H_2	2.5	1.89E-09	22.4	2	7.91E-09	29
CO_2	4	4.07E-08	7.5	3.8	8.23E-10	27
C_2H_4	2	9.07E-08	12.4	1.5	2.66E-09	26
C_2H_6	2.6	7.98E-10	21	1.6	1.36E-09	28

Langmuir-Freundlich fitting of adsorption isotherm for IAST selectivity calculation

The experimental data of pure component isotherms at 298 K for C_2H_2, CO_2, C_2H_4, C_2H_6 were fitted with the Langmuir-Freundlich model:

$$N = A_1 \frac{b_1 p^{c1}}{1 + b_1 p^{c1}} \quad \textbf{(Equation S4)}$$

where p (unit: kPa) is the pressure of the bulk gas at equilibrium with the adsorbed phase, N (unit: mmol/g) is the adsorbed amount per mass of adsorbent, A_1 (unit: mmol/g) is the saturation capacities, b_1 (unit: 1/kPa) is the affinity coefficients, and c_1 represents the deviation from an ideal homogeneous surface. Here, the single-component C_2H_2, CO_2, C_2H_4, and C_2H_6 adsorption isotherms have been fit to enable the application of IAST in simulating the performance of UTSA-220 under a mixed component gas. Adsorption isotherms and gas selectivity calculated by IAST for C_2H_2/CH_4 (1/99 v/v), C_2H_2/C_2H_4 (1/99 v/v), C_2H_2/C_2H_6 (50/50 v/v), C_2H_2/C_2H_4 (50/50 v/v) and C_2H_2/CO_2 (50/50 v/v) at 298 K in UTSA-220.

The selectivity of preferential adsorption of component *1* over component *2* in a mixture containing *1* and *2*, can be formally defined as:

$$S_{ads} = \frac{q_1/q_2}{p_1/p_2} \quad \textbf{(Equation S5)}$$

In the above equation, q_1 and q_2 are the absolute component loadings of the adsorbed phase in the mixture. These component loadings are also termed the uptake capacities. We calculate the values of q_1 and q_2 using the Ideal Adsorbed Solution Theory (IAST) of Myers and Prausnitz.

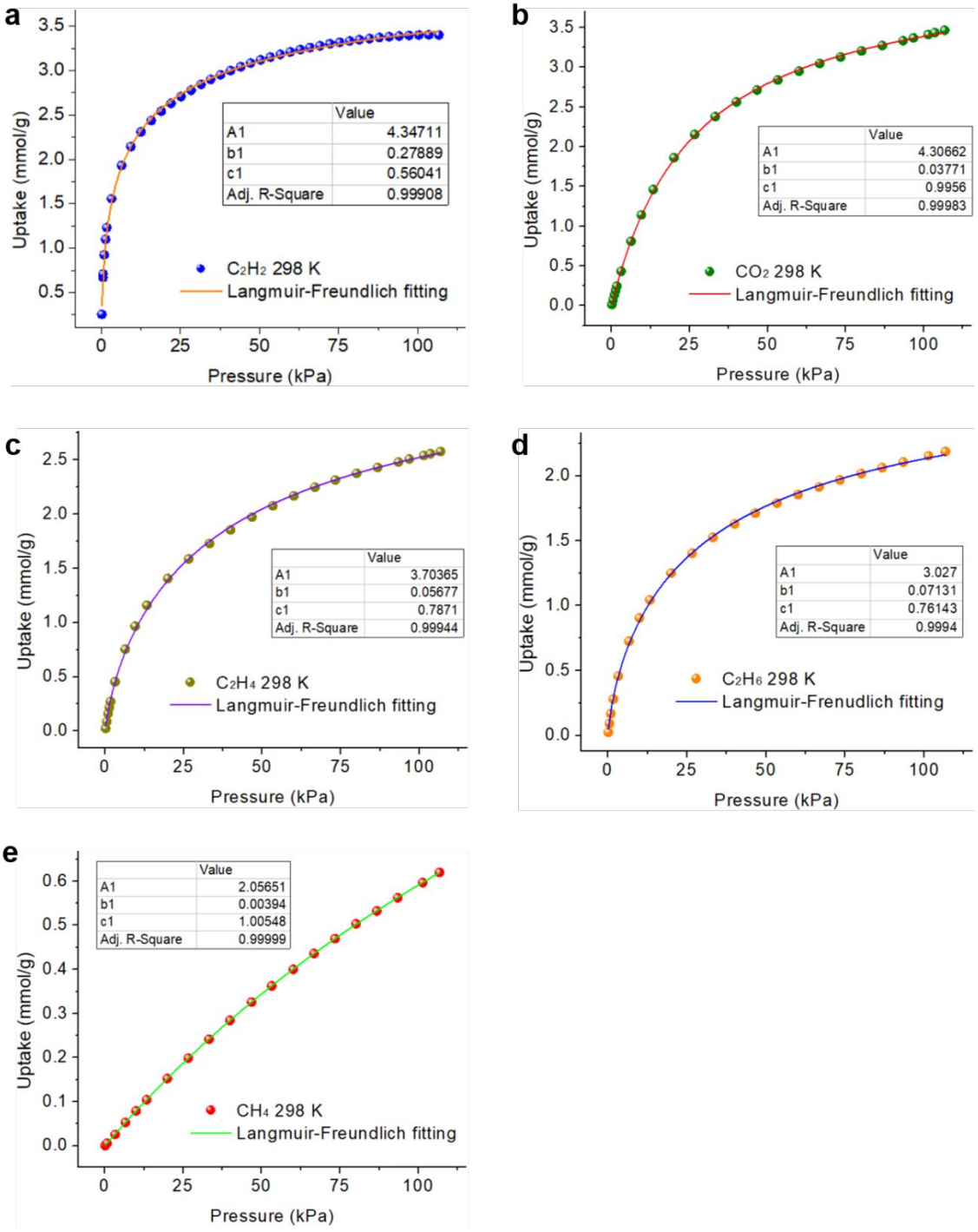

Figure S5. Langmuir-Freundlich fitting of (a) C_2H_2, (b) CO_2, (c) C_2H_4, (d) C_2H_6 and (e) CH_4 adsorption data of UTSA-220 at 298 K for IAST calculation. The resulting fitting parameters are listed in inset tables.

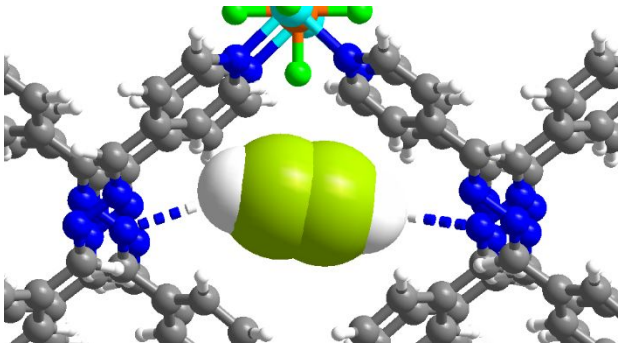

Figure S6. The DFT simulated extra binding site between C_2H_2 and azine group in UTSA-220. Atom color code: F, bright green; Si, orange; Cu, turquoise; C in framework, grey; C in adsorbed C_2H_2, lime; H, white; N, blue.

Breakthrough experiments

The experimental set-up consisted of two fixed-bed stainless steel columns. One column was loaded with the adsorbent (sample mass: 0.362 g), while the other was used as a blank control group to stabilize the gas flow. The flow rates of all gases mixtures were regulated by mass flow controllers, and the effluent gas stream from the column was detected by a gas chromatography (SHIMADZU GC-2014) with a thermal conductivity detector (TCD, detection limit 0.1 ppm).

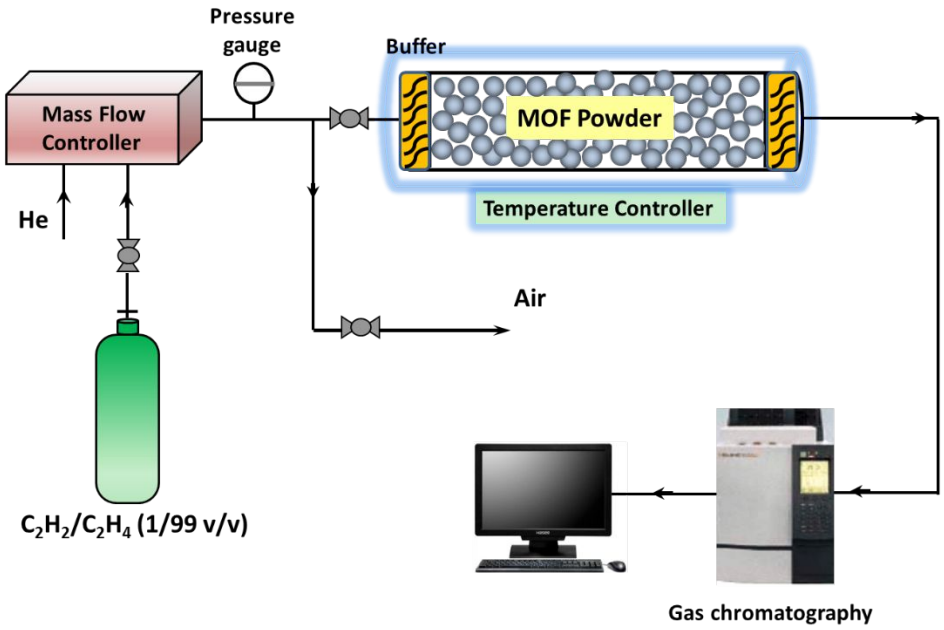

Figure S7. Illustration of the self-built breakthrough apparatus.

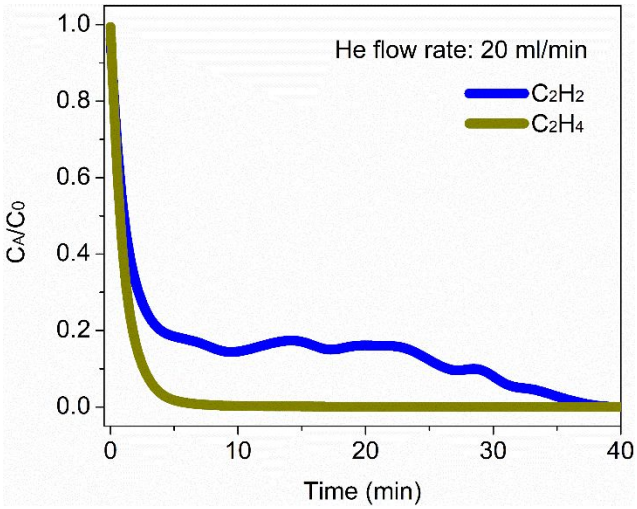

Figure S8. Concentration of C_2H_2 and C_2H_4 at the outlet when the column is purged with He (20 ml/min).

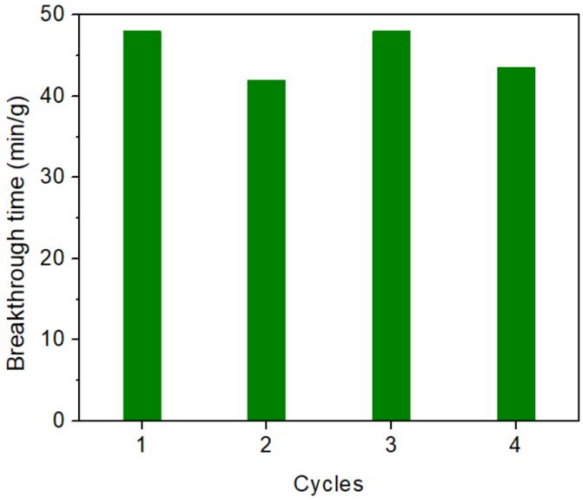

Figure S9. Breakthrough time of C_2H_2 in four experiment cycles.

Reference

1. Manna, B.; Sharma, S.; Ghosh, S. Synthesis and Crystal Structure of a Zn(II)-Based MOF Bearing Neutral N-Donor Linker and SiF_6^{2-} Anion. *Crystals* **2018**, *8* (1), 37.